Chapter-3

Ni stabilized Rock-Salt structured CoO; $Co_{1-x}Ni_xO$: Tuning of e_g electrons to Development a Novel OER Catalysts

3.1 Introduction

Efficient electrochemical energy generation, storage, and fuel production offer a clean alternative to fissile fuel combustion-based energy systems.[1–3] The oxygen evolution reaction (OER) is a key half-reaction in hydrogen-oxygen electrolyzers, rechargeable metal-air batteries, regenerative fuel cells such as solid oxide electrolyzer cells; SOECs. However, the OER suffers due to sluggish kinetics and the issue of overpotentials. To overcome the overpotential and sluggish kinetics of OER, efficient catalysts are required.[4–6] RuO_2 and IrO_2 are commonly considered benchmark electrocatalysts for OER owing to their high electrocatalytic activities toward OER in both acidic and alkaline solutions.[7-8] However, their low abundance, and high cost inhibit their practical usage. IrO_2 is the best electrocatalyst so far for OER. But, it is difficult to achieve dual activity; an acceptable limit of simultaneous OER and oxygen reduction reaction (ORR) activities. Therefore in recent years, the research drive is motivated toward the development of dual catalysts without the usage of noble/costly metals. The burgeoning efforts are taken by materials chemists to develop inexpensive materials with high electrocatalytic activity and stability for OER or preferably for both OER and ORR, it remains a daunting scientific challenge. However, recent studies show that the electrolysis of water is generally preferred in the alkaline medium over the acidic medium due to the higher stability of oxide materials towards corrosion.[9–11]

Transition metal oxides such as Co_3O_4,[12] MnO_2,[13] $NiCo_2O_4$,[14] $LaNiO_3$,[15] $LaCoO_3$,[16] and $SrCoO_{3-\delta}$ [17] in the form of Spinel and Perovskite structure are reported to exhibit real very good OER catalytic activity.[18] Several transition metal-containing perovskites were recently explored for the development of superior OER catalyst, and their activity was correlated with the applied potentials at a specific current density to

e_g electrons density present in the materials.[19] $Ba_{0.5}Sr_{0.5}Co_{0.8}Fe_{0.2}O_{3-d}$ (BSCF) was reported as the best OER catalyst with e_g electron (e_g = ~1.2) at the peak of the volcanic graph.[19] The systematic investigation of Co_3O_4-based Spinels, demonstrated the individual roles of Co^{2+} ions and Co^{3+} ions during OER and it was observed that Co^{2+} and Co^{3+} ions were differently responsible for OER activity in the Co_3O_4 system and confirmed that the divalent Co^{2+} dominated the OER activity.[20]

Perovskite and spinel-type structures accommodate transition metal ions in different oxidation states making it difficult to get a uniform Co^{2+} oxidation state across the structure with ~1.2 e_g electron. Here we envisaged Ni stabilized rock salt structured CoO in the form of $Ni_xCo_{1-x}O$ as a model host structure to tune the e_g electron concentration keeping the entire Co in a 2+ oxidation state. Here in this study, we present the stabilization of CoO in rock salt structure by doping Ni and study their electrocatalytic OER activity in alkaline media.

3.2 Materials Synthesis and characterizations

The solid-state ceramic synthesis route was used to synthesize crystalline Ni-doped cobalt oxides and the solid-state route in general results more thermodynamically stable compound. $Ni(OH)_2 \cdot NiCO_3 \cdot 4H_2O$ and $CoCO_3$ were taken as a suitable precursor because metathesis (simultaneous decomposition) of carbonates can result in solid solutions of Cobalt and Nickel oxides. The precursors are taken in stoichiometric ratio and mixed in agate mortar-pestle arrangement for about 40 minutes. The mixture is then fired at a temperature of 1050^oC for 12 hours. The sample was heated twice to get single-phase materials.

The phase formation was studied through Rigaku Miniflex desktop X-ray Diffractometer (XRD) with Cu-Kα radiation (λ = 1.54 Å) in the range 2θ ~ 20 - 90° with a step size of 0.02°. The structures were refined by the Rietveld refinement method using FULLPROF suite software and cubic CoO Rock salt structure (space group: Fm3m, No. 225) was taken as model structure. The microstructures of the sintered samples were investigated by using a scanning electron microscope (EVO - Scanning Electron Microscope MA15/18). The average grain size was calculated using the linear intercept method. The composition of the compounds was examined by Energy dispersive X-ray (EDX) spectroscopy with a probe attached to the scanning electron microscope. Infrared Spectra of the samples were recorded using Nicolet iS5

FTIR Spectrometer in the range of 400 to 4000 cm^{-1}. X-ray Photo-electron Spectroscopy (XPS) studies were carried out to investigate the electronic structure of the materials. XPS of the sample was carried out by Thermo Scientific Multilab 2000 instrument using Al Kα radiation operated at 150 W. Binding energies reported here are with reference to C (1s) at 284.5 eV and they are accurate within 0.1 eV.

3.2 .1 Electrochemical Studies

The electrochemical measurements were carried out using nova 2.0 autolab. The catalyst ink was prepared by homogenizing 12 mg of catalyst, 6 mg of carbon material, and 100 µL of Nafion®ionomer solution (0.26 mg mL^{-1}) in 3 mL of water under an ultrasonication bath for 40 min. To investigate the activity of the electrocatalyst, an aliquot of 10 µL of homogenized catalyst ink was deposited by a micropipette onto the surface of glassy carbon (GC) electrode with a geometric area of 7.06 mm^2, and the electrode was polished to a mirror-like appearance and dried under an IR lamp. The catalyst load was typically 566 µg cm^{-2} for the GC.

Linear sweep voltammetry (LSV), cyclic voltammetry (CV), and electrochemical impedance spectroscopy (EIS) in a conventional three-electrode arrangement were used to determine the electrochemical characteristics of the prepared electrocatalysts were measured by Metrohm Autolab (PGSTAT204) equipped with FRA32M module. Electrochemical measurements were analyzed using NOVA software.

Pt was used as a counter-electrode and Ag/AgCl in 3 M KCl was utilized as a reference electrode. All electrode potential values mentioned in this manuscript refer to this Ag/AgCl in the 3 M KCl electrode. Potential conversion for overpotential measurements was done using the following equation-

$$E_{RHE} = E_{Ag/AgCl} + E^{o}_{Ag/AgCl} + 0.059pH \quad (E^{o}_{Ag/AgCl} = 0.210 \text{ for 3 M KCl)} \quad (3.1)$$

$$\text{Overpotential} = E_{RHE} - 1.23 - iR \quad (3.2)$$

R is calculated using EIS measurements. Argon saturated 1-5 M KOH solution was used as the electrolyte. The electrolyte solutions were freshly prepared before each set of experiments from analytical grade KOH (Lachner, Czech Republic) and deionized water.

3.3 Results and Discussion

3.3.1 XRD and Crystal structure

Figure. 3.1(a) shows the XRD pattern of up to 50% Ni-doped Cobalt oxides. Except For Pure and 10% Ni-doped, Cobalt oxide $Co_{1-x}Ni_xO$ ($0 \leq x \leq 0.4$) peaks were identified for rock salt CoO structure, and for CoO and $Co_{0.9}Ni_{0.1}O$, small impurities peaks were identified for Spinel Co_3O_4 structure in the XRD pattern. With >10% Nickel doping, materials were synthesized in single-phase and all the diffraction peaks were identified only to rock salt structure. Therefore, it is clear from XRD studies that more than 10% Nickel substitution in cobalt oxide stabilizes the Rocksalt as ma ore thermodynamically stable structure. There is a continuous peak shift of (200) diffraction peaks with an increasing Nickel content in Cobalt oxide. Thus with increasing Nickel concentration, the peak shift of (200) diffraction peak toward higher 2θ indicates substitution incorporation of Ni ions into the CoO rock salt structure. The Rietveld refined XRD profile of $Co_{0.7}Ni_{0.3}O$ is shown in **Figure 3.1(b).** The observed intensities matched very well with the calculated intensities. The structural parameter derived for the refinement is given in **table 3.1**.
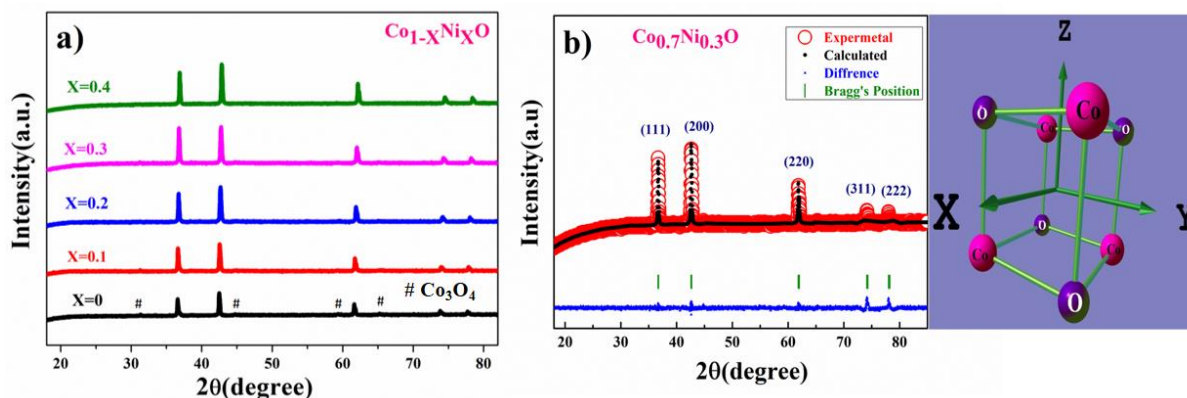

Figure 3.1 (a). X-ray diffraction patterns of Co_{1-x} Ni_xO ($0 \leq x \leq 0.4$) denoted (b). Rietveld refinement of XRD pattern of $Co_{0.7}Ni_{0.3}O$

Table 3.1: Structural Parameters of $Co_{1-x}Ni_xO$ ($0 \leq x \leq 0.4$)

Sample	a=b=c (A^0)	$\alpha=\beta,\gamma$ (^{0})	Chi^2	R_{bragg}	R_f	R_{wp}
$Co_{0.9}Ni_{0.1}O$	4.2479(3)	90	1.219	0.896	0.518	20.6
$Co_{0.8}Ni_{0.2}O$	4.2395(5)	90	.988	0.532	0.377	15.1
$Co_{0.7}Ni_{0.3}O$	4.2301(4)	90	1.15	1.87	1.57	20.7
$Co_{0.6}Ni_{0.4}O$	4.2242(3)	90	3.21	0.835	0.499	20.9

3.3.2 SEM analysis

SEM images in **Figure3. 2 (a-b)** clearly show the particle distribution and morphology of bulk 30% Ni-doped Cobalt oxide $Co_{0.7}Ni_{0.3}O$ microcrystals. The microcrystals are spherical and 2-5 micrometers in size. **Figure3.2(c)** shows the area of the sample on which EDX mapping was carried out to get the composition of the material. That data confirm that the composition of the materials (Ni: Co = 0.29±0.01: 0.7±0.01) is almost the same as the nominal composition utilized for the synthesis. EDX spectra. , EDX analysis shows the stoichiometric distribution of Co, Ni, and O elements.
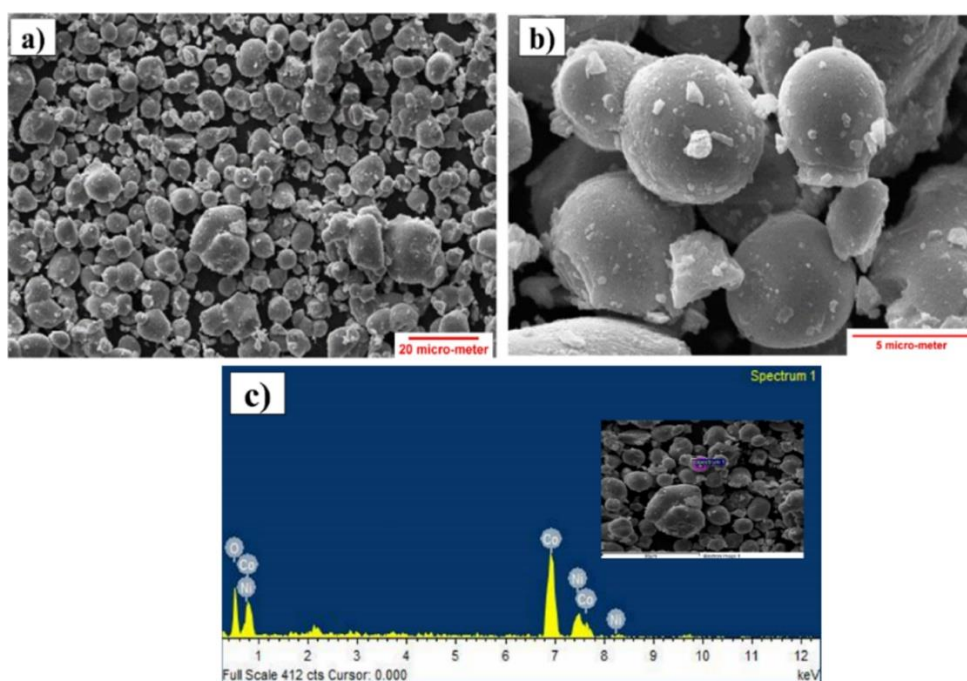

Figure 3.2 (a) Scanning electron micrograph of $Ni_{0.3}Co_{0.7}O$. (b) Scanning electron micrograph (enlarged view) of $Co_{0.7}Ni_{0.3}O$ (c) EDX analysis showing the stoichiometric distribution of Co, Ni, and O elements

3.3.3 Fourier transform infrared spectroscopy (FTIR) analysis

The FTIR spectrum of the $Co_{0.7}Ni_{0.3}O$ samples is shown in **Figure. 3.3** The absence of a peak at 3450 cm^{-1} (assigned to hydrogen-bonded hydroxyl stretching vibrations)[21] and the peak at 1630 cm^{-1} (attributable to H–O–H bending vibration mode) shows the absence of free water in the sample. The high-intensity peaks observed at 651 cm^{-1} and in the region of 407-558 cm^{-1} correspond to Ni-O and Co-O stretching and the Ni-OH and Co-OH bending respectively.[22-23] In general, the presence of Ni-OH bonding is known to enhance the OER activity of the sample.[24]
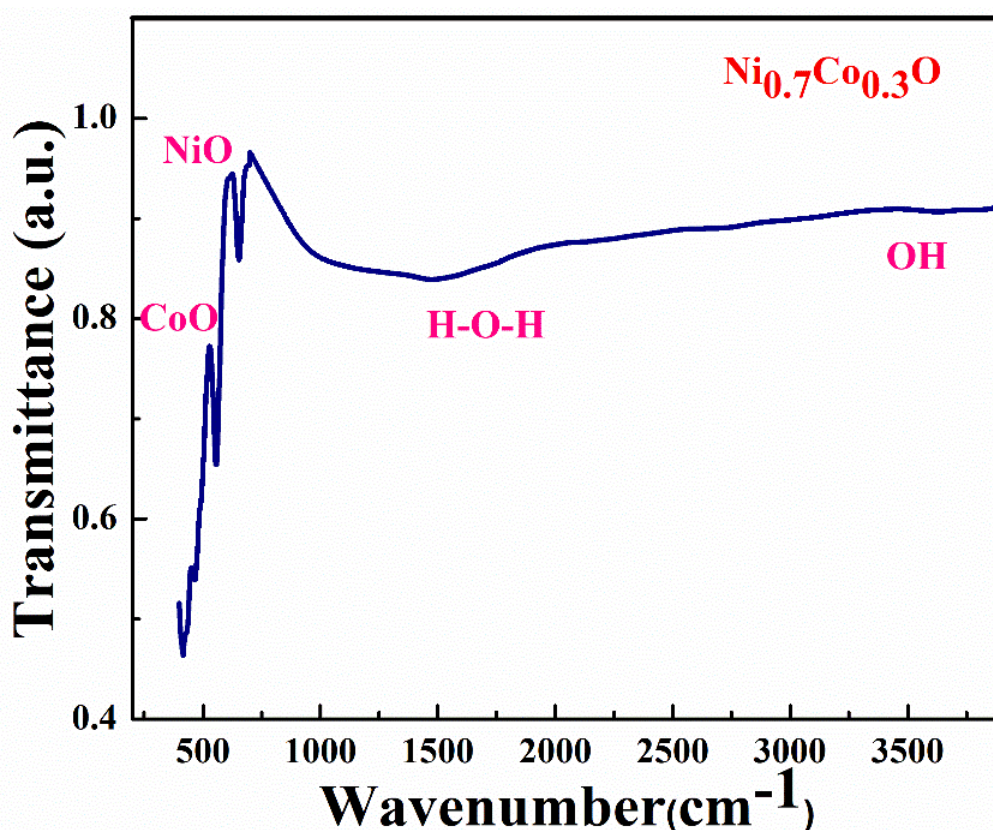
Figure 3.3 Fourier transform infrared spectroscopy (FTIR) spectrum of $Co_{0.7}Ni_{0.3}O$

3.3.4 X-ray photoelectron spectroscopy (XPS) analysis

XPS fitting measurements of core levels Ni (2p) and Co (2p) spectra of the $Co_{0.7}Ni_{0.3}O$ sample are shown in **Figure. 3**.4. **Figure 3.4 (a)**. shown full survey XPS of $Co_{0.7}Ni_{0.3}O$ power sample. The binding energy of 854.7 and 872.1 eV were observed for Ni $2p_{3/2}$ and Ni $2p_{1/2}$ peaks and satellite peaks were shown in 860.57eV and 878.48eV respectively in **figure 3.4 (b)**. The binding energies at 779.1 and 794.6

eV were observed for Co $2p_{3/2}$ and Co $2p_{1/2}$ peaks and satellite peaks were shown in 784.02 eV and 802.01eV respectively in **figure 3.4 (c)**. The binding energies at 528.4.1 and 530.59 eV were observed for lattice (O_2) O^{2-} and adsorbed $(O_2)O_2^{-2}/O^-$ peaks in **figure 3.4(d)**. These signal positions are typical for NiO and CoO and indicate the presence of Ni and Co atoms in the +2 oxidation state in the $Co_{0.7\ Ni0.3}O$ sample
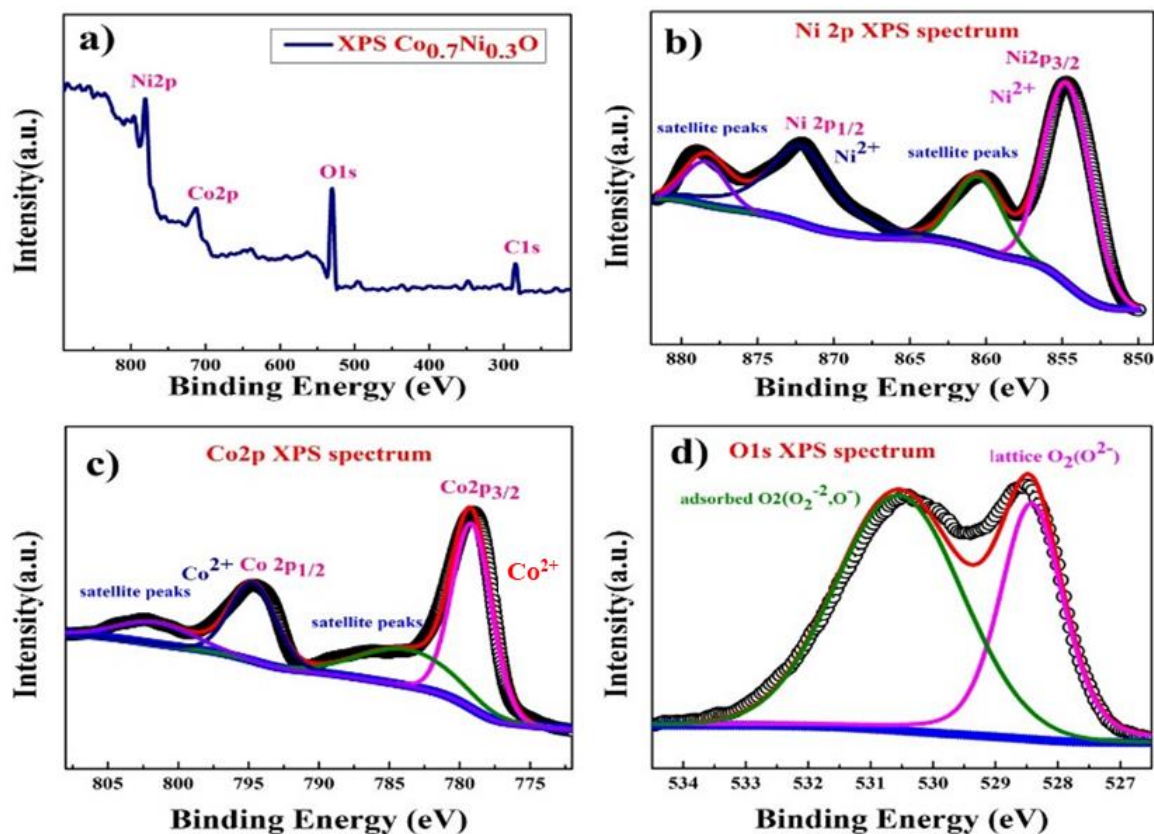

Figure 3.4 XPS of $Co_{0.7}Ni_{0.3}O$. (a) Full XPS survey of $Co_{0.7}Ni_{0.3}O$ (b) Core level Ni2p spectrum (c) Co2p spectrum (d) O1s spectrum

3.3.5 Linear Swept voltammetry (LSV) and Electrochemical Impedance Spectroscopy (EIS) analysis 1M KOH electrolyte

To know the electrochemical activities of different Ni-doped Cobalt oxides, Linear Sweep voltammetry was carried out with CoO to $Co_{0.5}Ni_{0.5}O$ samples in argon saturated 1M KOH electrolyte, and corresponding iR corrections were made according to EIS measurements (0.1 Hz to 1M Hz) shown in **figure 3.5(d).** The LSV

(Linear Swept voltammetry) was done at a 5mV/s scan rate and curves are shown in **Figure 3. 5(a -4b)** suggest that the highest current densities or the highest electro-catalytic activity for both OER and ORR were obtained for the $Ni_{0.3}Co_{0.7}O$ sample. The current densities for OER and ORR were on the rise with increasing doping concentration from CoO to $Co_{0.7}Ni_{0.3}O$ and drop significantly with further increase in Ni content, with $Co_{0.6}Ni_{0.4}O$ showing even lower catalytic activities than the undoped CoO sample. However, the catalytic activity of CoO was better than $Co_{0.9}Ni_{0.1}O$ in the case of OER and better than $Co_{0.9}Ni_{0.1}O$ and $Co_{0.8}Ni_{0.2}O$ in the case of ORR. This may be due to the presence of a minor spinel phase in the CoO and $Co_{0.9}Ni_{0.1}O$ samples.

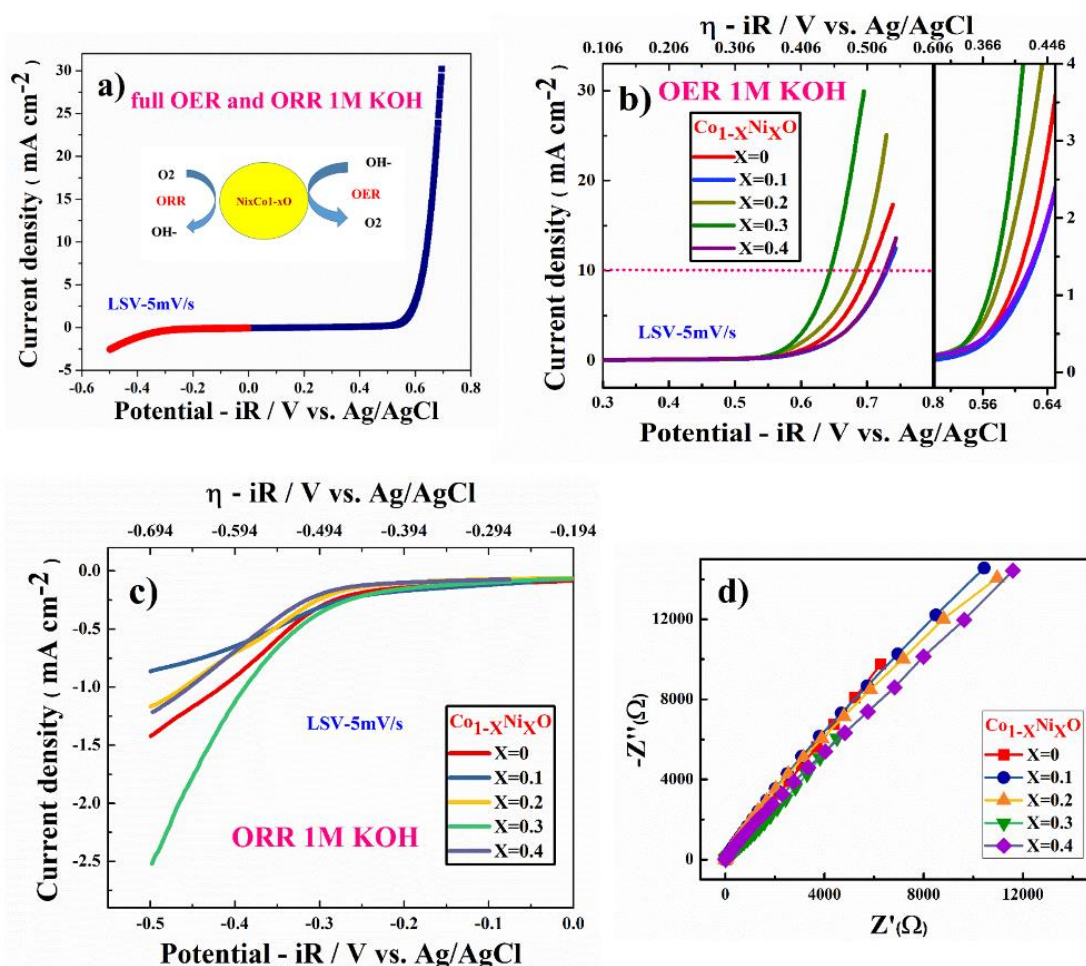**Figure. 3.5** (a) full OER and ORR performed of $Ni_{0.3}Co_{0.7}O$ with mechanism, (b)OER activity of $Co_{1-x}Ni_xO$ at 1 M KOH electrolyte at 5mV/s. (c) ORR activity of $Co_{1-x}Ni_xO$ at 1 M KOH electrolyte at 5mV/s. (d) EIS measurements of $Co_{1-x}Ni_xO$ at 1 M KOH electrolyte

As $Co_{0.7}Ni_{0.3}O$ performs superior electrochemical activity among all Ni-doped CoO samples in **Figure 3.5(c)**, To study the highest electrochemical performance of the materials, the catalytic ORR activities of $Co_{0.7}Ni_{0.3}O$ were also studied by varying the concentration of KOH electrolyte.

3.3.6 Linear Swept voltammetry (LSV) and EIS measurements in different molar KOH electrolyte

The OER activities increase with the increasing concentration of KOH electrolyte up to 5 molar concentration, and above 5M, the activity starts degrading as shown in **Figure. 3.6(a),** and corresponding iR corrections were made according to EIS measurements (0.1Hz to 1MZ) shown in **Figure 3.6(b)** The onset potential also decreases with the increases in the concentration of KOH electrolyte up to 5 molar solutions. Therefore, electrochemical activities of all Ni-doped samples were studied in 5M KOH electrolyte the highest catalytic activity was again confirmed for $Co_{0.7}Ni_{0.3}O$ sample for both OER and ORR as shown in
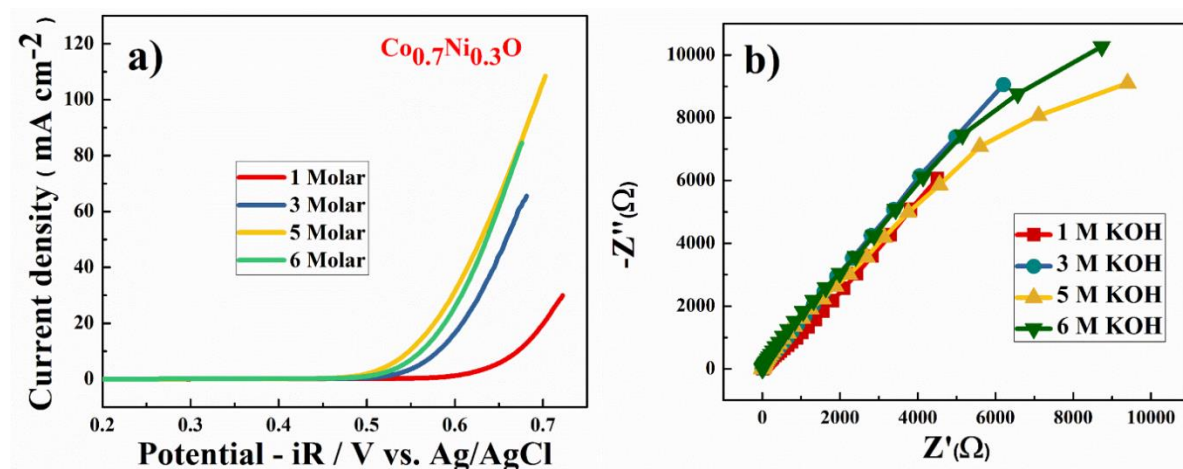

Figure. 3.6 (a) OER activity of $Co_{0.7}Ni_{0.3}O$ from 1M to 6 M KOH electrolyte (b) EIS measurements of $Co_{0.7}Ni_{0.3}O$ at different concentration KOH electrolyte

3.3.7 Linear Swept voltammetry (LSV) and EIS measurements in 5M KOH

In **Figure.3.7 (a-b),** the corresponding iR corrections were made according to EIS measurements shown in **Figure. 3.7(c).** We have observed that in OER and ORR studies, no redox peaks were observed confirming the non-capacitive behaviour and absence of high oxidation of Co and Ni in the form of M^{3+} as a higher oxidation state

undergoes redox transformation (M^{3+}/M^{2+}) that generates redox peak and capacitive storage.[25] The absence of a higher oxidation state (+3/+4) of Cobalt and Nickel in the $Ni_{0.3}Co_{0.7}O$ sample was also confirmed by the XPS studies. To understand the electrochemical activity of the material, the Tafel slope and overpotential play an important role. Table 3.2 shows the Tafel slope and overpotential value corresponding to 5M and 1M KOH respectively.
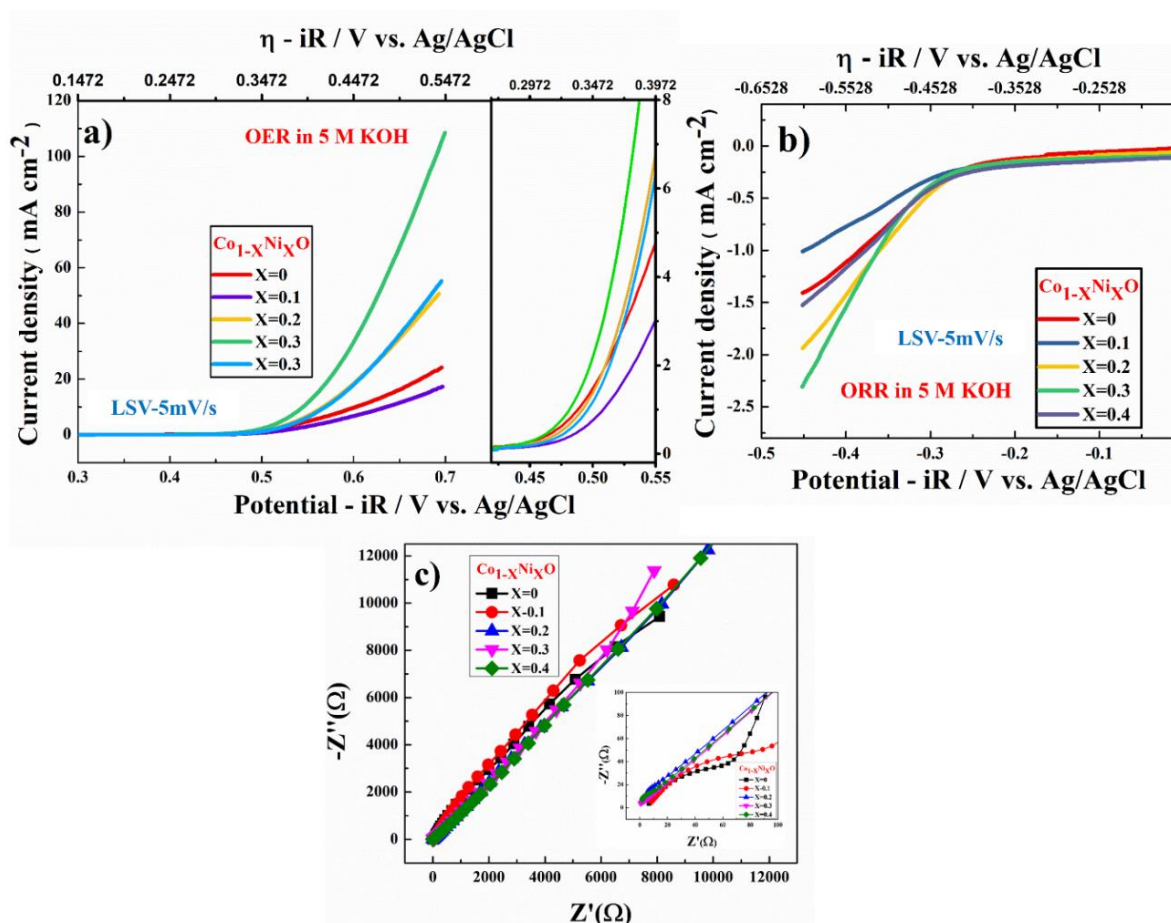

Figure.3.7 (a) OER activity of $Co_{1-x}Ni_xO$ at 5 M KOH electrolyte. (b) ORR activity of $Co_{1-x}Ni_xO$ at 5 M KOH electrolyte. (c) EIS measurements of $Co_{1-x}Ni_xO$ at 5 M KOH electrolyte.

3.3.8 Comparative Tafel slope in 1M and 5M KOH

The Tafel analysis at 1M KOH and 5M KOH concentration for $Co_{0.9\ Ni0.1}O$ to $Co_{0.6\ Ni0.4}O$ is shown in **Figure.3 8(a-b)**. A Low Tafel slope is usually an indication of a good electrocatalyst and the calculated Tafel slope values may provide insightful information about the reaction mechanism of the target system. Tafel slope values are given in Table 3.2 The general OER mechanism in alkaline solution on the metal site

(M) begins with a proton-coupled electron transfer from a surface-bound aqua species followed by an O−O the bond formation, [26-27] is described as follows:
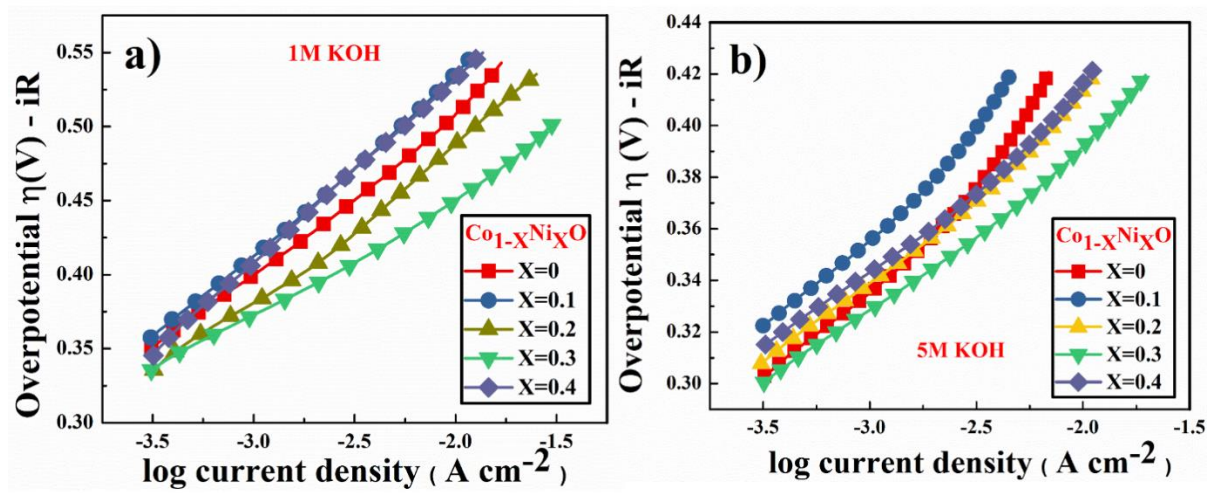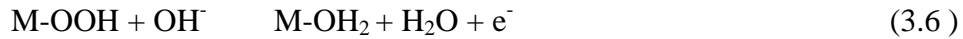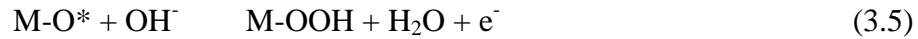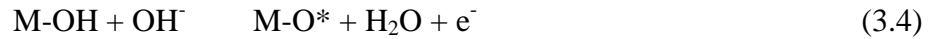
$$M\text{-}OH_2 + OH^- \quad M\text{-}OH + H_2O + e^- \quad\quad (3.3)$$

$$M\text{-}OH + OH^- \quad M\text{-}O^* + H_2O + e^- \quad\quad (3.4)$$

$$M\text{-}O^* + OH^- \quad M\text{-}OOH + H_2O + e^- \quad\quad (3.5)$$

$$M\text{-}OOH + OH^- \quad M\text{-}OH_2 + H_2O + e^- \quad\quad (3.6)$$
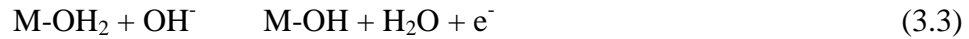
Figure. 3.8 (a) Tafel plot of $Co_{1-x}Ni_xO$ (0≤x≤0.4) at 1 M KOH. (b) Tafel plot of $Co_{1-x}Ni_xO$ (0≤x≤0.4) at 5 M KOH.

For the lower concentration of the electrolyte (1M), samples CoO, $Co_{0.9\ Ni0.1}O$, and $Co_{0.6\ Ni0.4}O$ show a Tafel slope close to the standard value of 96 mV dec^{-1}, 110 mV dec$^{-1,}$ and 122.2 mV dec^{-1} indicating that the OER process in CoO, $Co_{0.9}Ni_{0.1}O$, and $Co_{0.6}Ni_{0.4}O$ at 1M is limited at the first stage where the surface of catalyst was strongly bonded with −OH groups (reaction order = 1 with respect to OH$^-$ species with featured Tafel slope of 120 mV/dec).[28] Tafel slope of $Co_{0.8}Ni_{0.2}O$ and $Co_{0.7}Ni_{0.3}O$ was found to be 76 and 66.8 mV dec^{-1} which was very close to a featured Tafel slope of 60 mV/Dec. Therefore for $Co_{0.8\ Ni_{0.2}}O$ and $Co_{0.7}Ni_{0.3}O$ samples, the rate-determining step should be the H_2O removal and M-O* formation.[29] at the high concentration of electrolyte (5M), all the samples show a Tafel slope in the range of 57.93 to 70.41 close to a featured Tafel slope of 60 mV/Dec suggesting that at higher electrolyte concentration, the rate-determining step will be H_2O removal and M-O*

formation for all the materials. Thus The OER reactions for $Co_{0.7\ Ni0.3}O$ in aqueous 1-5M KOH electrolyte are controlled by the rate-determining step involving H_2O removal and M-O* formation as given in equation 3.2.[29] This suggests that with increasing OH⁻ or electrolyte concentration, electro-activity of the material will increase as demonstrated in our study. Once the entire adsorption site will be filled with OH⁻, the increase in the concentration of electrolyte will not affect the performance of the catalyst.

Table 3.2 Tafel slope and Overpotential values of $Co_{1-x}Ni_xO$ ($0 \leq x \leq 0.4$) at 1M and 5M KOH

Sample	Concentration	Overpotential at 10 mA cm^{-2}	Tafel slope mV dec^{-1}
CoO	1M KOH	0.50675	96.88
$Co_{0.9}Ni_{0.1}O$	1M KOH	0.5363	110.39
$Co_{0.8}Ni_{0.2}O$	1M KOH	0.48707	76
$Co_{0.7}Ni_{0.3}O$	1M KOH	0.45034	66.8
$Co_{0.6}Ni_{0.4}O$	1M KOH	0.53242	122.2
CoO	5M KOH	0.449	70.41
$Co_{0.9}Ni_{0.1}O$	5M KOH	0.48291	64.84
$Co_{0.8}Ni_{0.2}O$	5M KOH	0.4134	53.23
$Co_{0.7}Ni_{0.3}O$	5M KOH	0.389	52.34
$Co_{0.6}Ni_{0.4}O$	5M KOH	0.4165	57.93

3.3.9 Showing stability of OER catalyst in 5M KOH

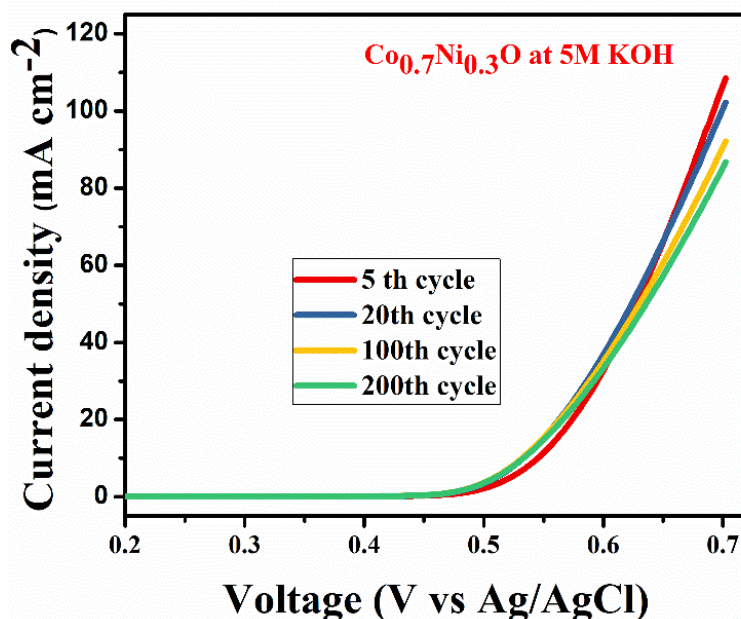**Figure 3.9** Showing stability of OER activity of $Co_{0.7}Ni_{0.3}O$ up to 200 cycles at 5mV/s.

The stability of the OER activity of the $Co_{0.7}Ni_{0.3}O$ catalyst is shown in **Figure. 3.9** The figure shows the LS curves after 5 cycles at 5 scan rates, 20 cycles at 5 scan rates, 100 cycles at 20 scan rates, and 200 cycles at 20 scan rates. In the first 20 cycles, the decrease in peak current was close to 5%, a further 10% of decrease was observed in 20th to 100 cycles and for 100 to 200 cycles almost 5% decrease was observed. Overall, $Ni_{0.3}Co_{0.7}O$ showed remarkably superior performance as an electrocatalyst for OER studies among all samples. The overpotential for the $Ni_{0.3}Co_{0.7}O$ sample was also found at ~0.450V for 1M and about ~0.389V at a 5M concentration of the KOH electrolyte. Recently, using DFT calculation it was shown that the over-potential for OER for a given electrocatalyst cannot be below 0.37V.[30-31] Observed overpotential (0.389V) of $Co_{0.7}Ni_{0.3}O$ at 5M electrolyte concentration is almost close to reaching the theoretical limit of 0.37V.

3.3.10 Role of e_g electrons on OER and ORR catalyst

Volcano graph depicting correlation of eg electrons with overpotential (at 10 mA cm-2) and the Tafel slope at 1 M KOH electrolyte. OER activity of different transition

metal-ions containing perovskites are established in their term of e_g electrons present in the compound and the volcano plot, it was established by Suntivich et al, that close to 1.25 e_g electrons, superior OER activity, and low overpotential can be achieved.[19] The superiority of Co^{2+} ions in higher OER activity was earlier confirmed by the comparative studies of $ZnCo_2O_4$, $CoAl_2O_4$, and Co_3O_4 in an aqueous KOH electrolyte.[32]
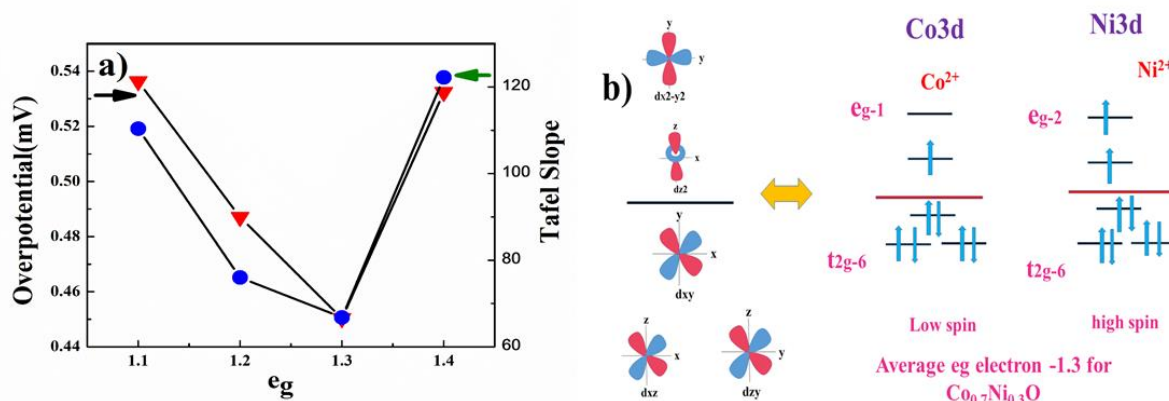

Figure 3.10 a) Volcano graph depicting correlation of eg electrons with overpotential (at 10 mA/ cm2) and the Tafel slope at 1 M KOH electrolyte b) d orbital presentation and e_g electron calculation

It was shown that in rock salt structured $NiCoO_2$ the Co^{2+} lies in the low spin $t_{2g}^6 e_g^1$ state and Ni^{2+} lies in the $t_{2g}^6 e_g^2$ state.[27] Thus, the total e_g electrons present in the compound can be varied from e_g^1 to e_g^2 from CoO to NiO. The volcano plat representing overpotential and Tafel Slope for e_g electron present in our samples are shown in **Figure 3.10 (a-b)**. It is evident from **Figure. 3.10. a)** that as the composition approaches $Co_{0.7}Ni_{0.3}O$ the overall e_g electrons approach 1.3 in the compound resulting from the higher OER activity.

3.4 Conclusions:

The rock-salt structure acted as a model host structure similar to perovskite where e_g electrons can be varied to obtain superior electro-catalytic activity. Incorporation of Nickel into CoO lattices helps to stabilize the rock salt structure and tune the e_g electrons to develop superior OER and ORR electrocatalysts. $Ni_{0.3}Co_{0.7}O$ with 1.3 e_g electrons showed superior electrocatalytic activity for oxygen evolution reaction. The overpotential for $Co_{0.7}Ni_{0.3}O$ sample was also found at ~0.45 V for 1M and about ~0.389 V at 5M concentration of the KOH electrolyte. The overpotential of the solid-state bulk synthesized rock salt $Co_{0.7}Ni_{0.3}O$ is found to be even lower than various nano-structured compounds like spinel Co_3O_4[33], and the catalytic activity is found to be even higher than that of the nano-structured $Co@N-C$[34] and $Co_{0.67}Ni_{0.33}S_2$ nanowire[35]. The catalytic activity of rock salt $Co_{0.7}Ni_{0.3}O$ is found to be better than both the rock salt parent oxide CoO (this work) and NiO [36]. This working model demonstrated a new area of tuning the e_g electrons in the rock salt structure similar to that Perovskite structure[14] The nano-engineering of designated material can further improve the activity of the materials and the study will be off very much interest.